Piotr RYBACKI, Zenon GRZEŚ
Uniwersytet Przyrodniczy w Poznaniu
Instytut Inżynierii Biosystemów
ul. Wojska Polskiego 50, 60-637 Poznań, Poland
e-mail: prybacki@up.poznan.pl;

Received: 2017-11-21 ; Accepted: 2018-01-23

IDENTIFICATION OF CAVITATION WEAR AREAS ON INNER LINING OF TUBES WITH VARIABLE RADIUS USING COMPUTER MODELING OF FLUID FLOW

Summary

The paper presents applicability of the computer system to model and simulate fluid and gas flow to assess surface cavitation wear. Abstract tube models with a decreasing inside diameter were developed and fluid flow with varying flow velocities was simulated. This facilitated identification of areas particularly at risk of cavitation wear. Results of simulation analyses were verified by comparing them with actual empirical results concerning cavitation erosion of tubing materials.
***Key words**: computer modeling, CAD/CAE, cavitation, erosion*

IDENTYFIKACJA OBSZARÓW ZUŻYCIA KAWITACYJNEGO WEWNĘTRZNYCH POWIERZCHNI PRZEWODÓW O ZMIENNEJ ŚREDNICY Z WYKORZYSTANIEM KOMPUTEROWEGO MODELOWANIA PRZEPŁYWU CIECZY

Streszczenie

W pracy przedstawiono możliwości wykorzystania systemów komputerowego modelowania oraz symulowania przepływu cieczy i gazów do oceny stopnia zużycia kawitacyjnego powierzchni. Opracowano abstrakcyjne modele przewodów o zmniejszającej się średnicy wewnętrznej oraz symulowano przepływ cieczy z różnymi prędkościami. Pozwoliło to wyznaczenie obszarów szczególnie narażonych na erozję kawitacyjną. Dokonano weryfikacji wyników analizy symulacyjnej porównując je z rzeczywistymi wynikami badań erozji kawitacyjnej materiałów do budowy przewodów.
***Słowa kluczowe**: kawitacja, erozja kawitacyjna, CAD/CAE, modelowanie komputerowe*

1. Introduction

Current studies on cavitation aim at the description of this phenomenon using e.g. other CAD/CAE systems. These systems may simulate fluid and gas flow conditions, while defining the type of materials and geometric parameters of tubes. Moreover, computer simulation to a considerable degree provides insight into phenomena accompanying kinematics and dynamics of fluid flow in hydraulic systems, a more precise determination of fluctuations in pressure and flow intensity, while it facilitates visualization of cavitation wear at rapid changes in pressure and energy of fluid particles [9, 16, 19, 20, 22, 24, 26].

The CAD/CAE systems make it possible to construct abstract models and automatic or semi-automatic simulation of mechanical load, strength of materials, heat exchange, distribution of radiation, fluid flow, assessment of durability and reliability of machines as well as the effect of physical phenomena on the intensity and wear of parts. Simulations within developed models make it possible to detect structural discontinuity as well as assembly errors and assembly collisions. They eliminate the need to construct physical models and thus reduce the time required and costs of launching new products on the market [5, 6, 8, 7, 9, 16, 19, 20, 22, 24, 26].

Cavitation is a common phenomenon observed when operating machines and hydraulic systems [4, 11, 13, 17, 18, 23, 25]. Despite intensive studies on the mechanism of its formation, numerous questions arise concerning the effect of cavitation erosion on the structure of tubing materials and the dynamics of changes in parameters of flowing fluid or gas.

Dular et al. [4], Niederhofer et al. [11] and Wójs [21] presented an opinion that cavitation is caused by a variable pressure field in the fluid and consists in the formation, growth and dissipation of bubbles or other enclosed spaces (cavities), containing vapor of a given fluid, dissolved gases or vapor-gas mixtures. Behbahani-Nejad [1], Dular et al. [4] and Li et al. [10] stated in their publications that bubbles increase in size in the areas of pressure reduced below a critical value and next they rapidly decrease in the areas of pressure exceeding the critical value. The critical pressure value depends on the type and temperature of fluid, contents of dissolved and undissolved gases and solid particles, the state of fluid movement, the manner of cavitation development as well as the thermodynamic state of the fluid defining the rate of their enucleation, i.e. the number and type of cavitation nuclei.

Cavitation results in numerous effects, which in the opinion of many researchers may be divided into primary and secondary [4, 11, 18, 25]. The best known symptom of cavitation is manifested in cavitation noise, resulting from bubble implosion, increasing with the development of cavitation and transformed into static within a wide frequency range of 102-105 Hz. The impact of pressure impulses on the walls, caused by implosion of bubbles, generates additional noise and vibrations of the entire hydraulic system. Cavitation promotes dissipation of energy, which is manifested in hydraulic systems in the form of increased losses, while in hydraulic machines it leads to reduced capacity, lifting height, efficiency, etc. In the area of bubble and cavity dissipation the temperature increases and in some cases cavitation is accompanied by luminescence, such as gas luminescence during implosion of cavitation bubbles. In the

area of reduced pressure the fluid is degassed. Intensive cavitation results in the dispersion of chemical agents, degradation of high molecular weight polymer additives, etc. Literature sources also mention other primary effects, e.g. changes in electrical conductance of the fluid and electric potential, changes in the heat transfer coefficient, etc. [4, 11, 18, 21, 25].

According to Wójs [21], secondary cavitation effects include first of all disturbance or changes in the material structure of walls limiting the cavitation areas, caused by the mechanical impact of a high pressure fluid or locally by very high temperature, oxidation, diffusion, etc.

In terms of energy the cavitation intensity index is the power per unit area of a material, as specified in the formula proposed by Thiruvengadan [14, 15, 21]:

$$\overline{P} = \frac{P}{A}, \tag{1}$$

where: P is the power absorbed by a material with the surface area A.

Brinkhorsta et al. [2] in their study proposed a method to determine cavitation erosion intensity by calculating cavitation index σ according to the following formula:

$$\sigma = \frac{p_2 - p_v}{p_1 - p_2}, \tag{2}$$

where: p_v is the value of pressure of saturated vapor of a fluid, p_1 is the initial value of fluid pressure and p_2 is the value of pressure at the analyzed point of the tube.

2. The aim, scope and methods of analyses

The aim of the study was to identify cavitation wear areas on inner surface of tubes with variable cross-section diameter using computer modeling of water flow. Based on recorded water parameters and on the dependence developed by Brinkhorsta et al. [2] cavitation index σ was determined for characteristic points of the tested tube.

The scope of the study comprises the construction of an abstract tube model, within which a narrowed tube diameter was designed, decreasing from d_{m1} = 25 mm to d_{n1} = 10 mm and characteristic points were established based on the Cartesian coordinate system, whose origin was established on the contraction plane, i.e. at point x = 0, y = 0, z = 0 (Fig. 1).

In order to provide a more comprehensive analysis of water flow and changes in its parameters in the developed abstract model three variants of orifice edge roundness were modelled in the contraction plane, i.e. r_1 = 0 mm, r_2 = 1 mm and r_3 = 2 mm (Fig. 2a, 2b, 2c).

Simulation experiments were conducted at the laminar water flow towards positive values of the z axis of the Cartesian coordinate system. Flowing water velocity ranged from 5 to 100 m·s^{-1}.

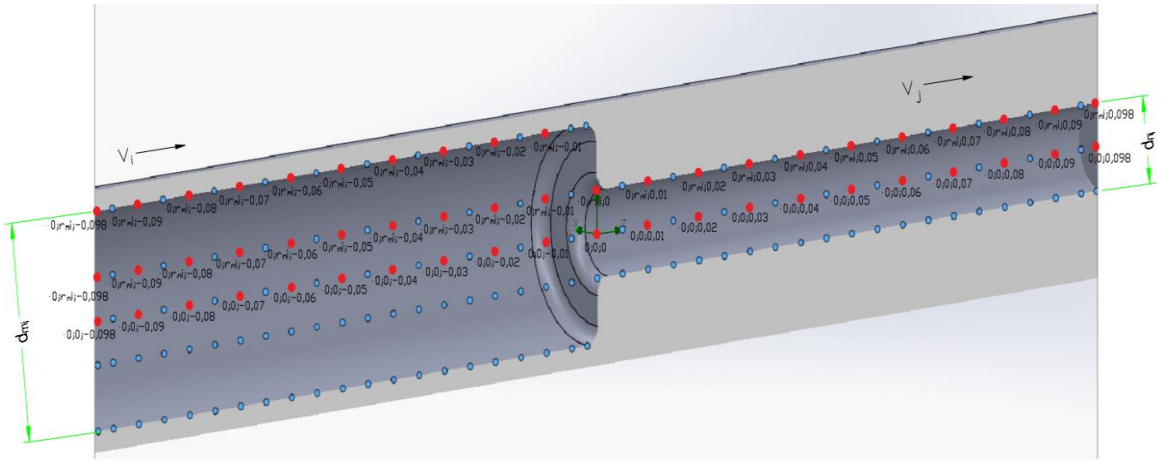

Source: own work / Źródło: opracowanie własne

Fig. 1. An abstract model of a tube with a change in inside diameter and established measurement points for flowing water parameters

Rys. 1. Model abstrakcyjny przewodu ze zmianą średnicy wewnętrznej oraz wyznaczonymi punktami analizy parametrów przepływającej wody

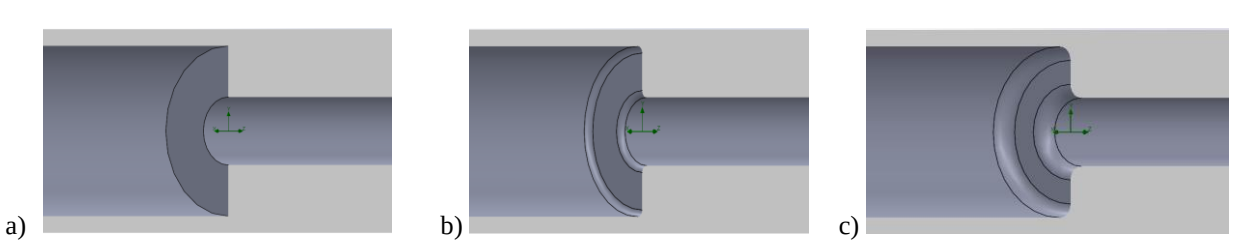

Source: own work / Źródło: opracowanie własne

Fig. 2. Reduction in inner tube diameter from 25 mm to 10 mm for various values of orifice edge radius: a) r_1 = 0 mm, b) r_2 = 1 mm and c) r_3 = 2 mm

Rys. 2. Redukcja średnicy wewnętrznej przewodu z wymiaru 25 mm do 10 mm, dla różnych wartości zaokrąglenia krawędzi zwężenia: a) r_1 = 0 mm, b) r_2 = 1 mm, c) r_3 = 2 mm

3. Simulation experiments and discussion of their results

During fluid flow within the area of a rapid change in the cross-section diameter the jet is additionally narrowed under the influence of forces of inertia [12, 21]. As it is shown in Fig. 3 being a visualization of CAD water flow simulation, fluid within the area of field changes fills the entire tube cross-section, whereas the flowing jet fills only its part, with the rest of the cross-section filled by recirculation zones.

In their studies Brinkhorsta et al. [2] and Cioncolini et al. [3] reported that at the maximum contraction of the jet pressure decreases as a result of increased flow velocity and energy losses. Bubbles of gas may be formed then, which after penetrating to areas with elevated pressure undergo rapid implosion. If this takes place on the wall surface, fluid hits metal. The higher the temperature of the fluid, the more likely it is for cavitation to develop. According to Brinkhorsta et al. [2] and Wójs [21], it results from empirical data that the condition for the development of cavitation may be presented as $p_{\min} \leq p_{kr}$, where p_{kr} is the critical pressure value, at which cavitation bubbles of fluid are formed. Knowing values of pressure p_{min} and areas where it is found in tubes it is possible to determine intensity of cavitation erosion processes.

Fig. 4 presents a visualization of water flow at the initial velocity 5 m·s^{-1} through a tube with a reduced diameter and orifice edge radius r_1 = 0 mm, as well as values of parameters at characteristic points of that tube. It results from simulation processes that flow velocity in the tube contraction plane at the origin of the coordinate system increases to 29.99 m·s^{-1}, with the highest value of 45.73 m·s^{-1} observed at the point with the coordinates $x = 0$, $y = 0$, $z = 0.01$.

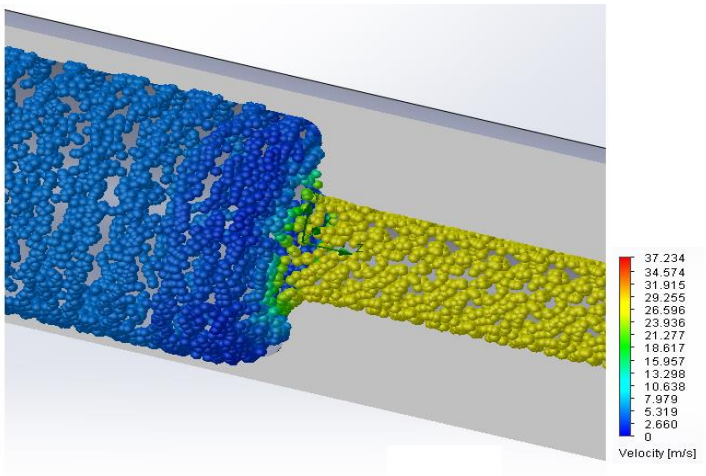

Source: own work / Źródło: opracowanie własne

Fig. 3. Visualization of water jet flow with initial velocity 5 m·s^{-1} and reduction in tube diameter from 25 mm to 10 mm
Rys. 3. Wizualizacja przepływu strugi wody z początkową prędkością 5 m·s^{-1} i redukcją średnicy przewodu z wymiaru 25 mm do 10 mm

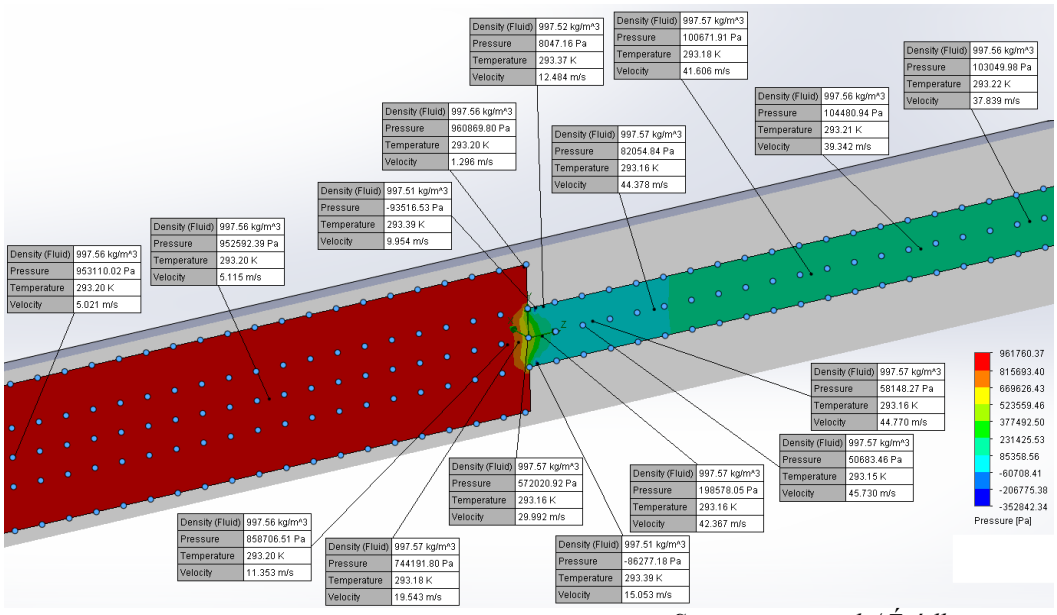

Source: own work / Źródło: opracowanie własne

Fig. 4. Visualization of parameters of water flow through a tube with diameter reduction and initial velocity of 5 m·s^{-1} and with orifice edge radius r_1 = 0 mm
Rys. 4. Wizualizacja parametrów przepływu wody przez przewód z redukcją średnicy i początkową prędkością 5 m·s^{-1} oraz zaokrągleniem krawędzi zwężenia r_1 = 0 mm

Water pressure at the origin reaches 953.11 kPa, while at the contraction plane its value decreased to 572.02 kPa. At the point of $x = 0$, $y = 0$, $z = 0.01$, where the greatest flow velocity was recorded, pressure reached 50.68 kPa. The lowest pressure (-93.52 kPa) at the assumed parameters was found at the point with coordinates $x = 0$, $y = 0.05$ and $z = 0.005$. The ratio of minimum pressure p_{min} to initial pressure p_0 in the analyzed case of laminar water flow is -0.09.

In the simulation of water flow the areas, in which pressure increased, were also observed. For example, at the point of $x = 0$, $y = 0.0125$ and $z = 0$, where flow velocity was 1.30 m·s^{-1}, the value of water pressure is 960.87 kPa. In turn, the ratio of maximum pressure p_{max} to initial pressure p_0 was 1.01.

Results obtained using computer simulation of water flow are consistent with empirical data in this respect [2]. For this reason computer simulation facilitates precise, rapid and cheap identification of locations and values of reduction in pressure of the flowing fluid. This method makes it possible to determine the areas and intensity of cavitation erosion in tested tubes.

From the point of view of fluid flow kinematics and dynamics an important problem in the case of a sudden contraction, narrowing of the tube diameter, is connected with the shape of the edge in the contraction plane. The developed abstract model was modified using CAD systems by changing the tube contraction edge radius and water flow was simulated under such conditions.

Figs. 5 to 7 present the distribution of pressures in a tube with changing diameters and various orifice edge radius values ($r_1 = 0$ mm, $r_2 = 1$ mm, $r_3 = 2$ mm) at a water flow velocity of 10 m·s^{-1}. Areas of a rapid pressure drop are evident, mainly at tube walls in the initial length of the contraction segment. Based on the computer simulation of water flow it may be observed that an increase in orifice edge radius causes smaller reductions of water flow pressure.

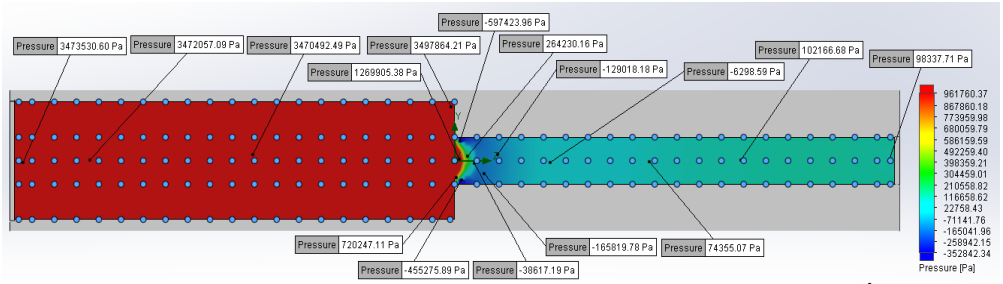

Source: own work / Źródło: opracowanie własne

Fig. 5. Distribution of water pressure values with characteristic points of analysis (flow velocity 10 m·s^{-1}, orifice edge radius $r_1 = 0$ mm)

Rys. 5. Rozkład wartości ciśnienia wody z charakterystycznymi punktami analizy (prędkość przepływu 10 m·s^{-1}, zaokrąglenie krawędzi zwężenia $r_1 = 0$ mm)

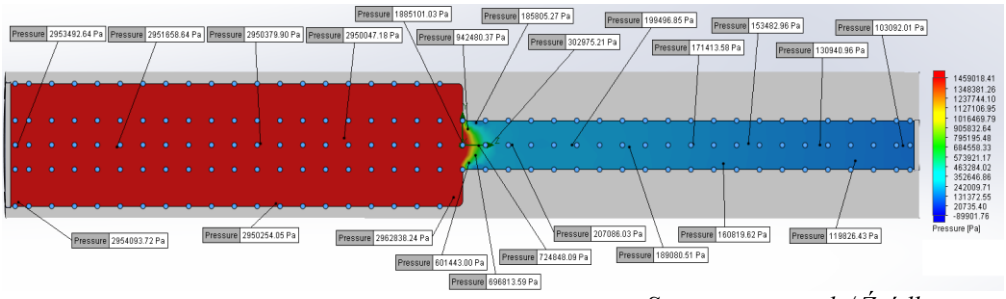

Source: own work / Źródło: opracowanie własne

Fig. 6. Distribution of water pressure values with characteristic points of analysis (flow velocity 10 m·s^{-1}, orifice edge radius $r_1 = 1$ mm)

Rys. 6. Rozkład wartości ciśnienia wody z charakterystycznymi punktami analizy (prędkość przepływu 10 m·s^{-1}, zaokrąglenie krawędzi zwężenia $r_1 = 1$ mm)

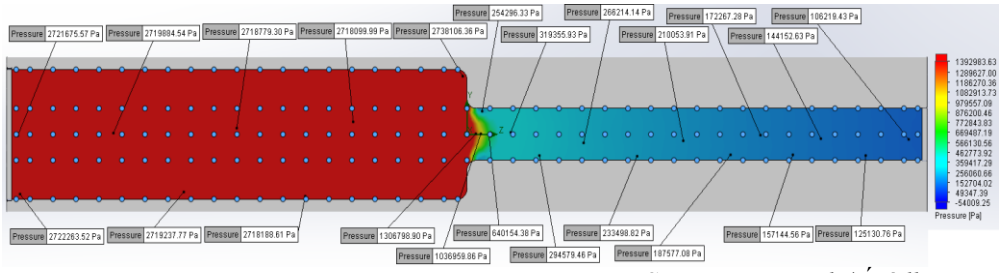

Source: own work / Źródło: opracowanie własne

Fig. 7. Distribution of water pressure values with characteristic points of analysis (flow velocity 10 m·s^{-1}, orifice edge radius $r_1 = 2$ mm)

Rys. 7. Rozkład wartości ciśnienia wody z charakterystycznymi punktami analizy (prędkość przepływu 10 m·s^{-1}, zaokrąglenie krawędzi zwężenia $r_1 = 2$ mm)

Precise pressure distribution values for the developed models at water flow with velocities ranging from 5 to 100 $m \cdot s^{-1}$ along the axis from the adopted coordinate system are presented in Figs. 8 to 10. Irrespective of the tested model a greater decrease in pressure was observed with an increase in fluid flow velocity. The greatest decrease and the development of negative pressure of -39.88 MPa and at the same time the greatest intensity of cavitation processes were recorded at the tube wall segment between coordinates x = 0, y = 0.05, z = 0 and x = 0, y = 0.05, z = 0.05, at a water flow velocity of 100 $m \cdot s^{-1}$ in the model with orifice edge radius $r_1 = 0$ mm. The ratio of minimum pressure p_{min} to initial pressure p_0 in the analyzed case of laminar water flow was -0.12.

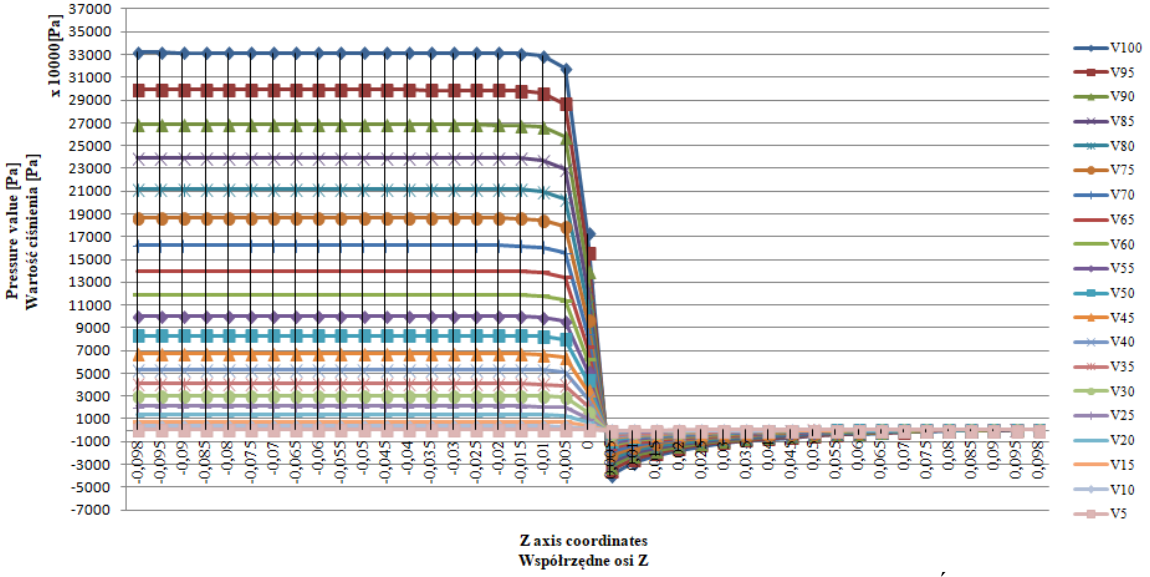

Source: own work / Źródło: opracowanie własne

Fig. 8. Water pressure at tube contraction from 25 mm to 10 mm and orifice edge radius r_1 = 0 mm (Cartesian system coordinates x = 0, y = 0.05, z = from -0.098 to 0.098)

Rys. 8. Wartości ciśnienia wody w warunkach redukcji średnicy przewodu z wymiaru 25 mm do 10 mm i zaokrągleniu krawędzi zwężenia r_1 = 0 mm (współrzędne układu kartezjańskiego x = 0; y = 0,05; z = od -0,098 do 0,098)

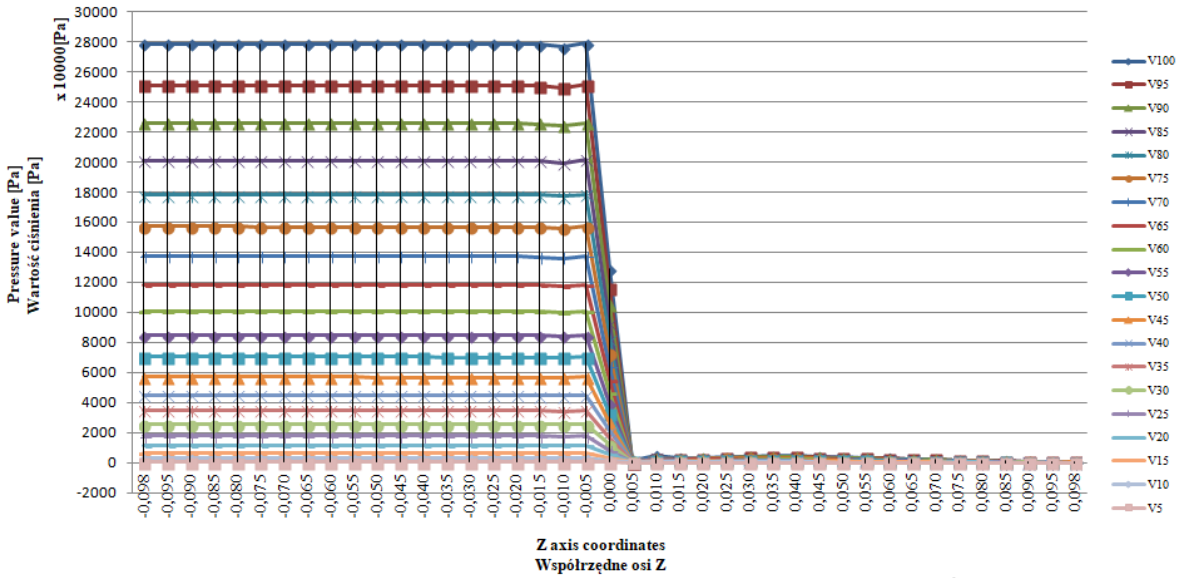

Source: own work / Źródło: opracowanie własne

Fig. 9. Water pressure at tube contraction from 25 mm to 10 mm and orifice edge radius r_1 = 1 mm (Cartesian system coordinates x = 0, y = 0.05, z = from -0.098 to 0.098)

Rys. 9. Wartości ciśnienia wody w warunkach redukcji średnicy przewodu z wymiaru 25 mm do 10 mm i zaokrągleniu krawędzi zwężenia r_1 = 1 mm (współrzędne układu kartezjańskiego x = 0; y = 0,05; z = od -0,098 do 0,098)

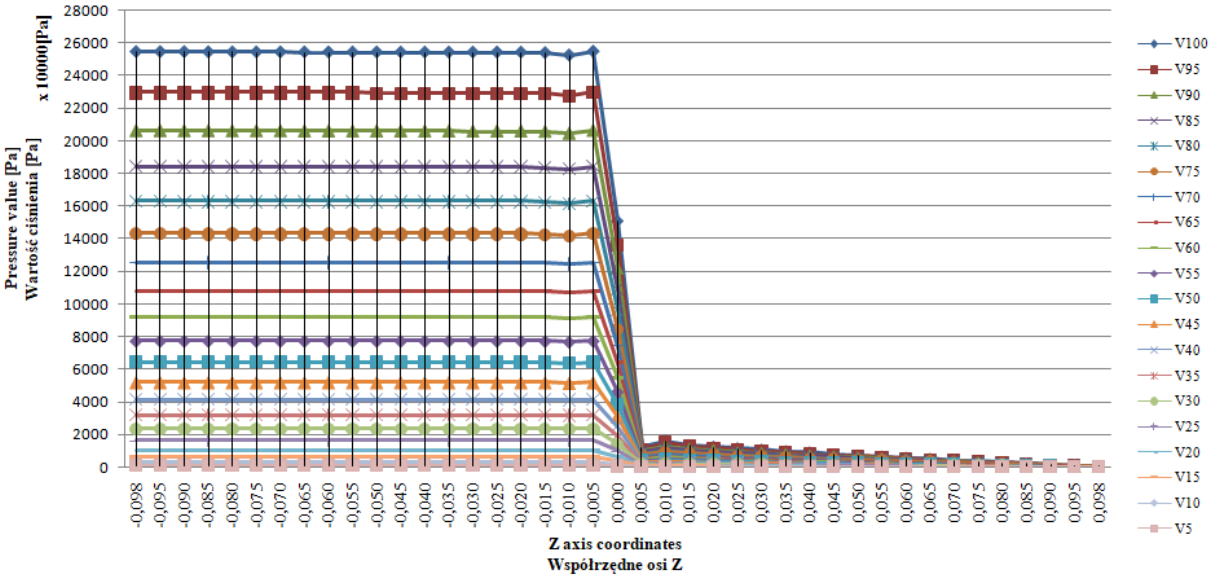

Source: own work / Źródło: opracowanie własne

Fig. 10. Water pressure at tube contraction from 25 mm to 10 mm and orifice edge radius r_1 = 2 mm (Cartesian system coordinates x = 0, y = 0.05, z = from -0.098 to 0.098)

Rys. 10. Wartości ciśnienia wody w warunkach redukcji średnicy przewodu z wymiaru 25 mm do 10 mm i zaokrągleniu krawędzi zwężenia r_1 = 2 mm (współrzędne układu kartezjańskiego x = 0; y = 0,05; z = od -0,098 do 0,098)

Based on the results of computer simulations the reduction in water pressure was observed to be smaller in the case of models with rounded edges in the cross-section contraction plane. Based on the tube with contraction orifice radius r_2 = 1 mm, in which water flows at 100 m·s^{-1}, water pressure as a result of its increased velocity decreased to 0.45 MPa, while the ratio of minimum pressure p_{min} to initial pressure p_0 was 0.01.

We also need to focus on the results concerning energy of the flowing water jet. The greatest value of 6.8 kJ·kg^{-1} was recorded at water flow velocity of 100 m·s^{-1} in the tube with orifice edge radius r_1 = 0 mm (Fig. 11). In the case of the same flow velocity in the tube with orifice edge radius r_2 = 1 mm, the maximum water jet energy was 3.7 kJ·kg^{-1} (Fig. 12). In turn, in the tube with orifice edge radius r_3 = 2 mm the maximum water jet energy was 1.4 kJ·kg^{-1} (Fig. 13). Presented results clearly show that even a slight modification of inner edges of a tube reduces water jet energy. Moreover, this modification results in the transfer of its maximum value farther from the diameter reduction plane and its distribution over a longer tube section.

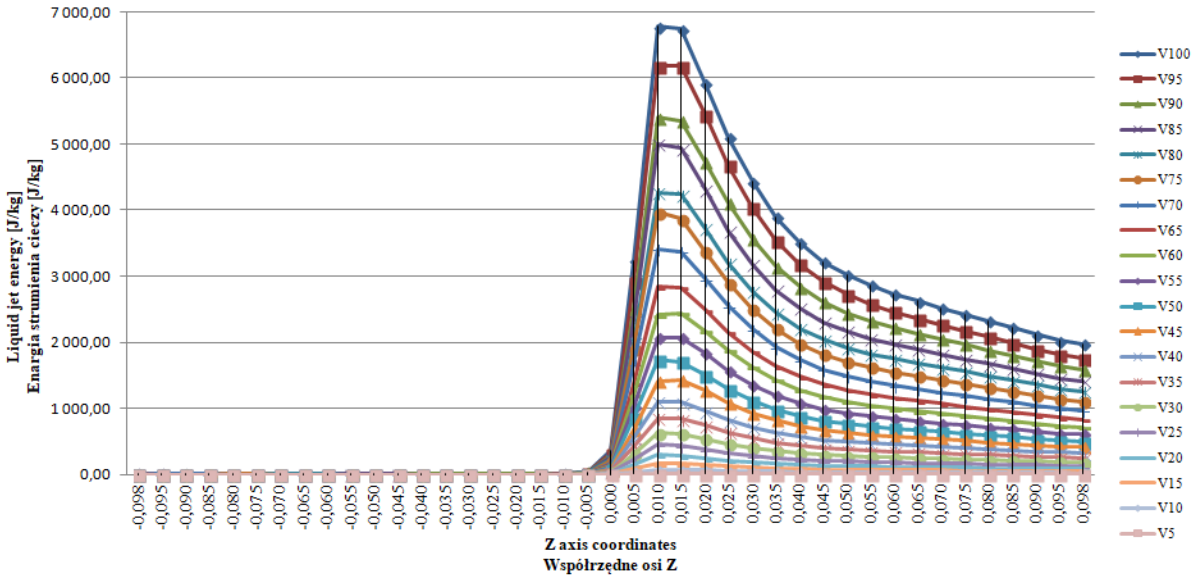

Source: own work / Źródło: opracowanie własne

Fig. 11. Values of water jet energy at tube contraction from 25 mm to 10 mm and orifice edge radius r_1 = 0 mm (Cartesian system coordinates x = 0, y = 0.05, z = from -0.098 to 0.098)

Rys. 11. Wartości energii strumienia wody w warunkach redukcji średnicy przewodu z wymiaru 25 mm do 10 mm i zaokrągleniu krawędzi zwężenia r_1 = 0 mm (współrzędne kartezjańskiego układu x = 0; y = 0,05; z = od -0,098 do 0,098)

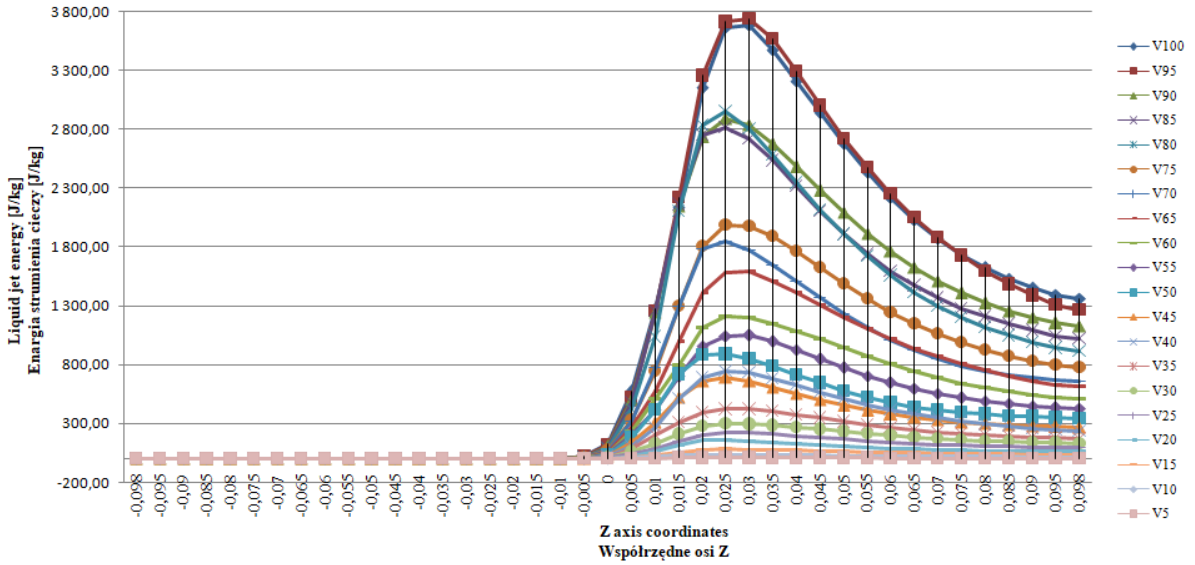

Source: own work / Źródło: opracowanie własne

Fig. 12. Values of water jet energy at tube contraction from 25 mm to 10 mm and orifice edge radius r_1 = 1 mm (Cartesian system coordinates x = 0, y = 0.05, z = from -0.098 to 0.098)

Rys. 12. Wartości energii strumienia wody w warunkach redukcji średnicy przewodu z wymiaru 25 mm do 10 mm i zaokrągleniu krawędzi zwężenia r_1 = 1 mm (współrzędne kartezjańskiego układu x = 0; y = 0,05; z = od -0,098 do 0,098)

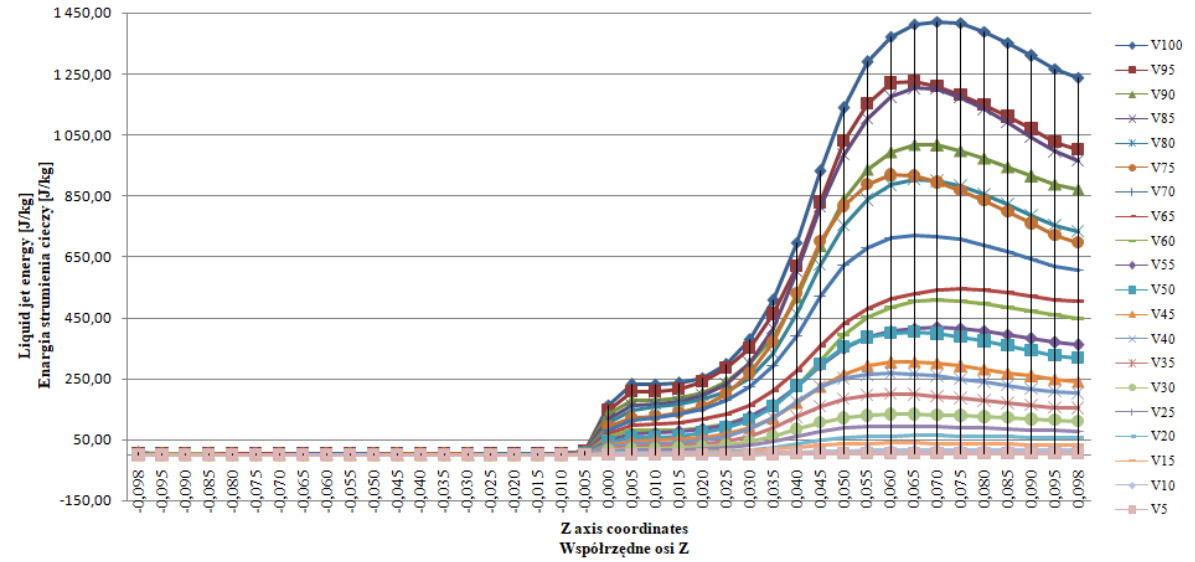

Source: own work / Źródło: opracowanie własne

Fig. 13. Values of water jet energy at tube contraction from 25 mm to 10 mm and orifice edge radius r_1 = 2 mm (Cartesian system coordinates x = 0, y = 0.05, z = from -0.098 to 0.098)

Rys. 13. Wartości energii strumienia wody w warunkach redukcji średnicy przewodu z wymiaru 25 mm do 10 mm i zaokrągleniu krawędzi zwężenia r_1 = 2 mm (współrzędne kartezjańskiego układu x = 0; y = 0,05; z = od -0,098 do 0,098)

In the presented fluid flow simulation the initial water temperature was assumed at 293.15 K. Water temperature changed depending on the adopted orifice roundness variant and water pressure values. The greatest changes in water temperature were observed in the abstract model of a tube with contraction orifice radius r_1 = 0 mm. In this case at the section with coordinates from z = -0.02 to z = -0.005 water temperature increased to 297.22 K, which was connected with an increase in pressure at the flow velocity of 100 m·s^{-1}. Next as a result of expansion water temperature decreased to 275.08 K at the point with coordinates x = 0, y = 0, z = 0 (Fig. 14). A characteristic point of the tested tube is that with coordinates x = 0, y = 0, z = 0.075, in which irrespective of flow velocity water temperature is 293.15 K.

A greater stability within the range of water temperatures may be observed for the abstract model of a tube with contraction orifice edge radius r_2 = 1 mm. The maximum temperature of 296.00 K was recorded at the point with coordinates x = 0, y = 0, z = -0.005, while the minimum temperature of -283.55 K was observed at the point of x = 0, y = 0, z = 0.01 for water flow velocity of 100 m·s^{-1} (Fig. 15).

The greatest stability of temperature for water flowing with a velocity of 100 m·s^{-1} was found for a tube with contraction orifice radius r_3 = 2 mm. The maximum water temperature (295.84 K) was observed at the point with coordinates x = 0, y = 0, z = -0.005, while the minimum temperature (285.36 K) was recorded at the point of x = 0, y = 0, z = 0.05 (Fig. 16).

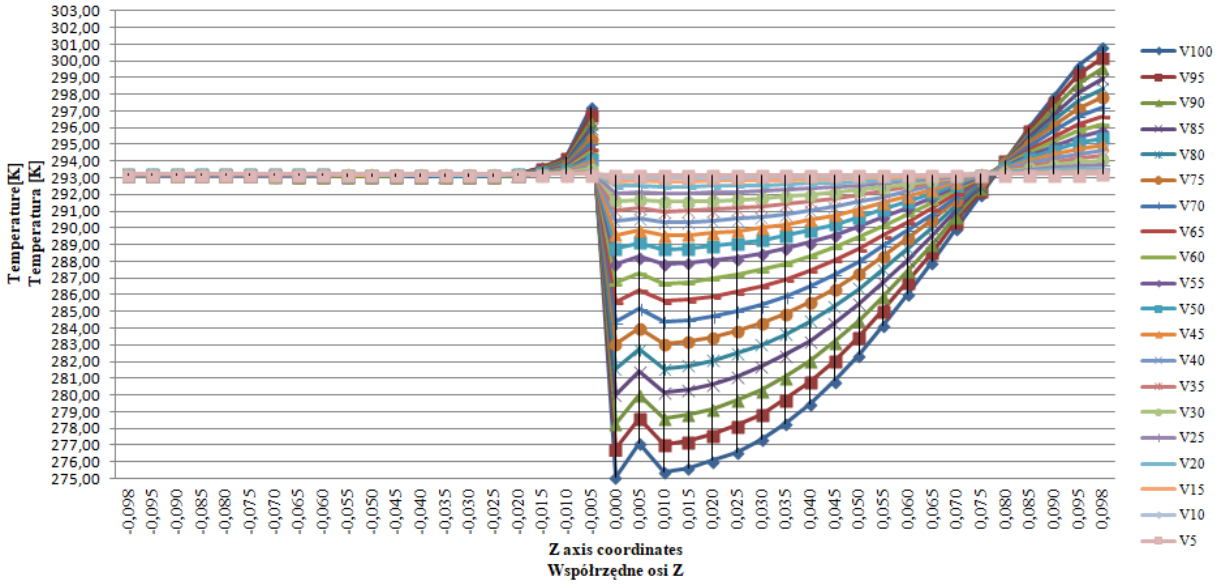

Source: own work / Źródło: opracowanie własne

Fig. 14. Water jet temperature at tube contraction from 25 mm to 10 mm and orifice edge radius r_1 = 0 mm (Cartesian system coordinates x = 0, y = 0.05, z = from -0.098 to 0.098)

Rys. 14. Wartości temperatury strumienia wody w warunkach redukcji średnicy przewodu z wymiaru 25 mm do 10 mm i zaokrągleniu krawędzi zwężenia r_1 = 0 mm (współrzędne układu kartezjańskiego x = 0; y = 0,05; z = od -0,098 do 0,098)

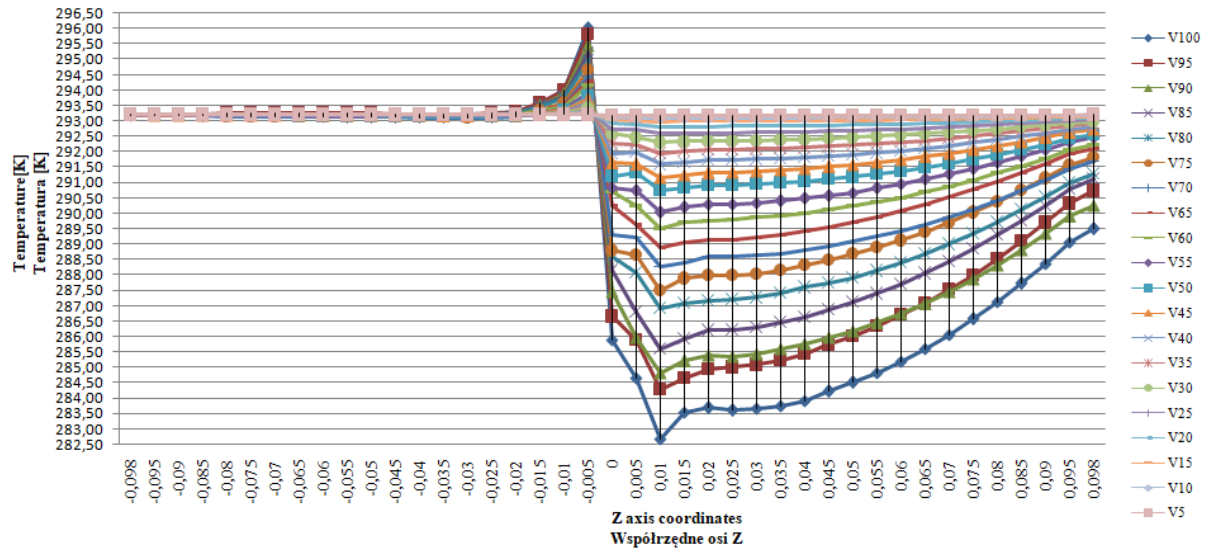

Source: own work / Źródło: opracowanie własne

Fig. 15. Water jet temperature at tube contraction from 25 mm to 10 mm and orifice edge radius r_2 = 1 mm (Cartesian system coordinates x = 0, y = 0.05, z = from -0.098 to 0.098)

Rys. 15. Wartości temperatury strumienia wody w warunkach redukcji średnicy przewodu z wymiaru 25 mm do 10 mm i zaokrągleniu krawędzi zwężenia r_2 = 1 mm (współrzędne układu kartezjańskiego x = 0; y = 0,05; z = od -0,098 do 0,098)

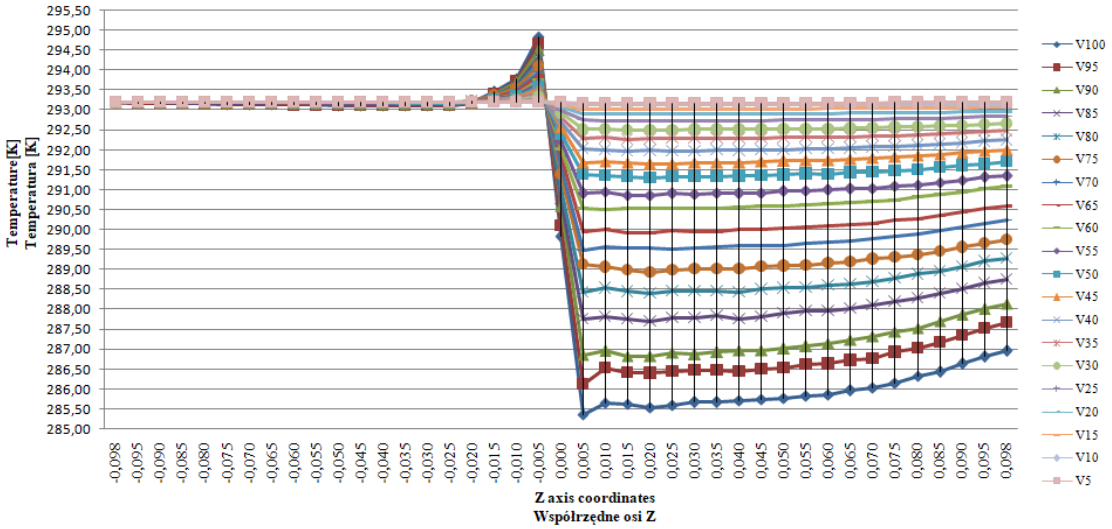

Source: own work / Źródło: opracowanie własne

Fig. 16. Water jet temperature at tube contraction from 25 mm to 10 mm and orifice edge radius r_3 = 2 mm (Cartesian system coordinates x = 0, y = 0.05, z = from -0.098 to 0.098)

Rys. 16. Wartości temperatury strumienia wody w warunkach redukcji średnicy przewodu z wymiaru 25 mm do 10 mm i zaokrągleniu krawędzi zwężenia r_3 = 2 mm (współrzędne układu kartezjańskiego x = 0; y = 0,05; z = od -0,098 do 0,098)

From the point of view of studies on fluid flow an essential problem is connected with the value of the Prandtl number, expressing the ratio of water momentum viscosity to its thermal diffusivity. In this study computer simulation was used to determine the value of the Prandtl number for analyzed variants of the abstract model of a tube with a contraction (reduction of the inside diameter) of the cross-section plane.

In the model developed for a tube with a contraction orifice edge radius r_1 = 0 mm at a water flow velocity of 100 m·s^{-1} value of the Prandtl number decreases to 5.67 at the point with coordinates x = 0, y = 0, z = -0.005. Next it rapidly increases to the maximum value of 12.59 at the point of x = 0, y = 0, z = 0.01, followed again by a decrease in the Prandtl number (Fig. 17). Moreover, it was observed that in the tested tube there is a point with coordinates x = 0, y = 0, z = 0.08, in which the Prandtl number is constant (7.00) irrespective of water flow velocity.

A smaller amplitude of changes in the Prandtl number was obtained in the computer simulation of water flow through a tube with contraction orifice radius r_2 = 1 mm (Fig. 18). For the comparable water flow velocity (100 m·s^{-1}) the minimum value of the Prandtl number is 5.85 in the point with coordinates x = 0, y = 0, z = -0.005, while the maximum value of 9.59 was recorded at x = 0, y = 0, z = 0.01.

The greatest stability of the Prandtl number values was obtained at the simulated water flow velocity of 100 m·s^{-1} through a tube with a contraction orifice edge radius r_3 = 2 mm (Fig. 19). In that case the minimum value of the Prandtl number is 6.04 at the point with coordinates x = 0, y = 0, z = -0.005, while the maximum value of 8.74 was recorded at x = 0, y = 0, z = 0.01.

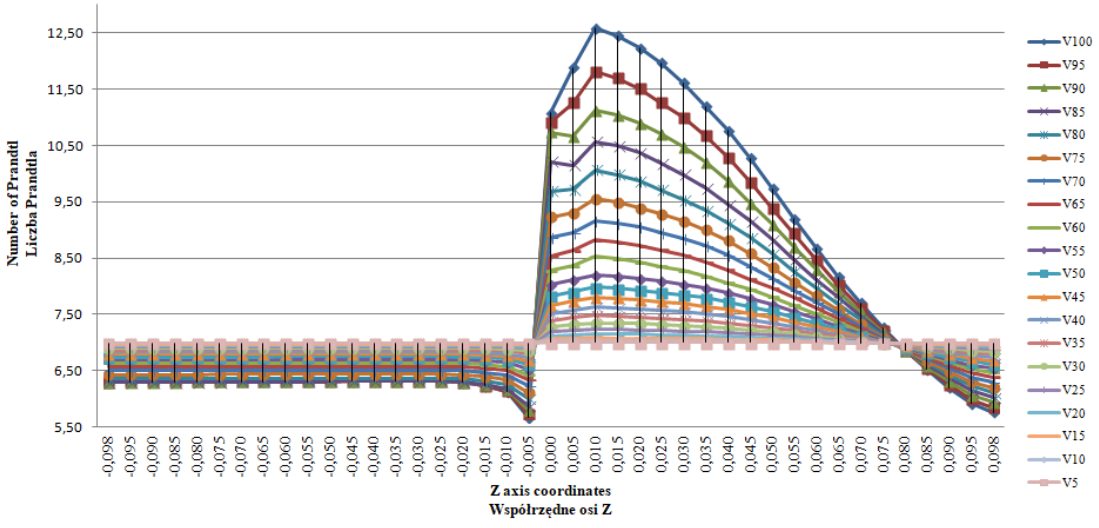

Source: own work / Źródło: opracowanie własne

Fig. 17. Values of the Prandtl number for water jet at tube contraction from 25 mm to 10 mm and orifice edge radius r_1 = 0 mm (Cartesian system coordinates x = 0, y = 0.05, z = from -0.098 to 0.098)

Rys. 17. Wartości liczby Prandtla strumienia wody w warunkach redukcji średnicy przewodu z wymiaru 25 mm do 10 mm i zaokrągleniu krawędzi zwężenia r_1 = 0 mm (współrzędne układu kartezjańskiego x = 0; y = 0,05; z = od -0,098 do 0,098)

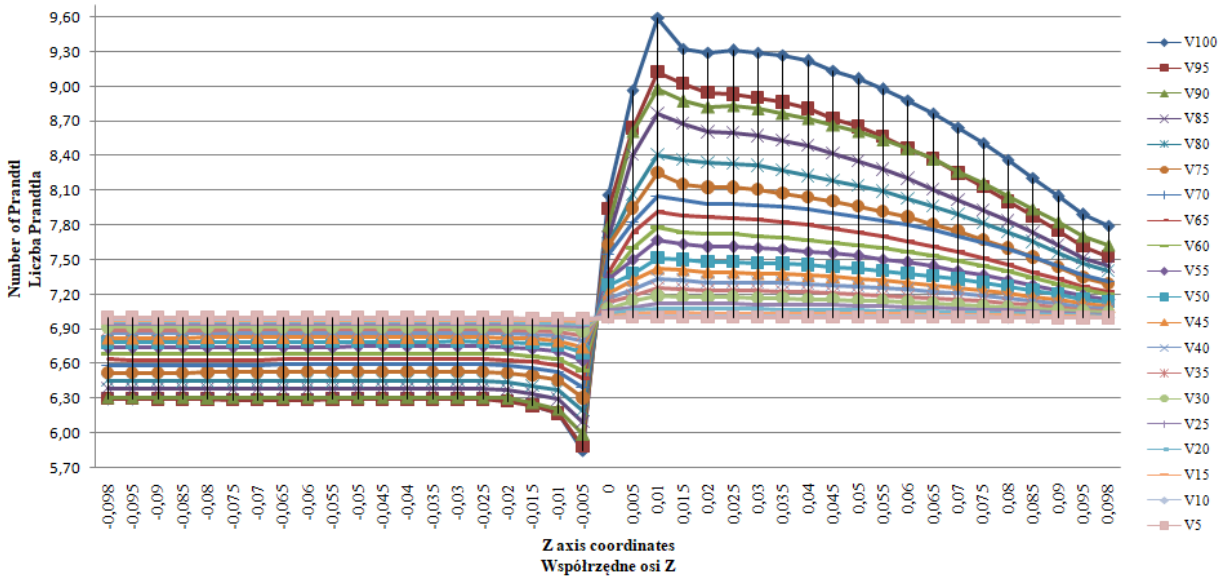

Source: own work / Źródło: opracowanie własne

Fig. 18. Values of the Prandtl number for water jet at tube contraction from 25 mm to 10 mm and orifice edge radius r_2 = 1 mm (Cartesian system coordinates x = 0, y = 0.05, z = from -0.098 to 0.098)

Rys. 18. Wartości liczby Prandtla strumienia wody w warunkach redukcji średnicy przewodu z wymiaru 25 mm do 10 mm i zaokrągleniu krawędzi zwężenia r_2 = 1 mm (współrzędne układu kartezjańskiego x = 0; y = 0,05; z = od -0,098 do 0,098)

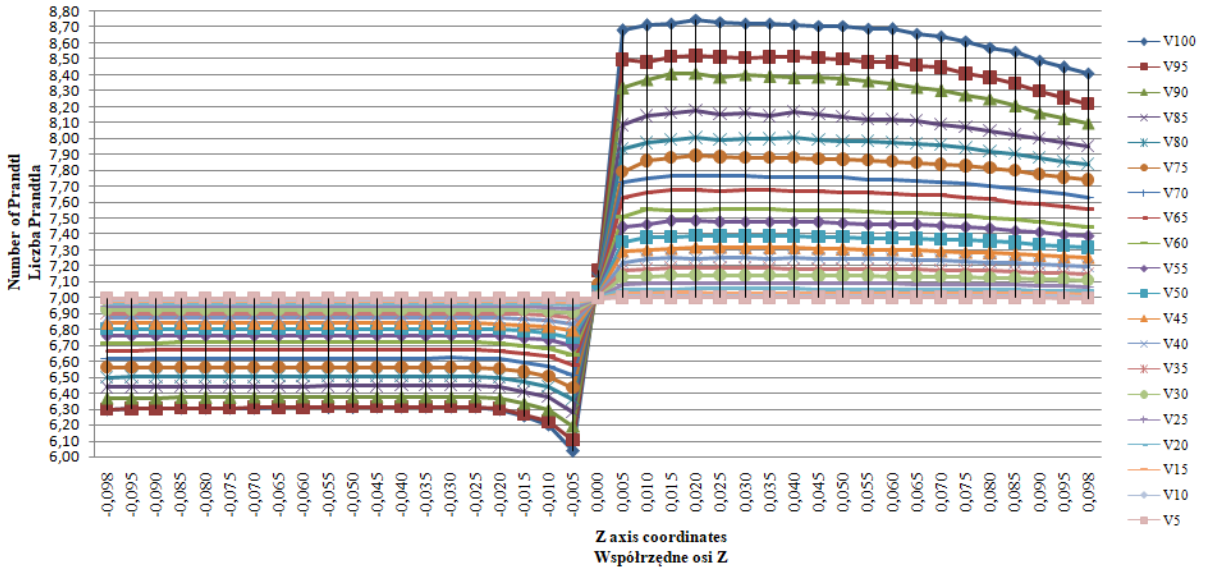

Source: own work / Źródło: opracowanie własne

Fig. 19. Values of the Prandtl number for water jet at tube contraction from 25 mm to 10 mm and orifice edge radius r_3 = 2 mm (Cartesian system coordinates x = 0, y = 0.05, z = from -0.098 to 0.098)

Rys. 19. Wartości liczby Prandtla strumienia wody w warunkach redukcji średnicy przewodu z wymiaru 25 mm do 10 mm i zaokrągleniu krawędzi zwężenia r_3 = 2 mm (współrzędne układu kartezjańskiego x = 0; y = 0,05; z = od -0,098 do 0,098)

Parameter values of fluid flow through a tube with inside diameter contraction, presented in this study based on water flow, make it possible to implement the equation proposed by Brinkhorsta et al. [2] and determine the intensity of cavitation erosion. For that purpose cavitation index σ was established, which is a measure of cavitation wear for the tested tube. Values of that index for the investigated abstract model are presented in Fig. 20. As it may be seen from the course of the function, they depend on water flow velocity and on the angle of tube contraction edge roundness. At a lower water flow velocity (up to 20 m·s^{-1}) values of cavitation index σ are comparable, while above the velocity of 25 m·s^{-1} the σ index values vary. This may indicate a diverse intensity of water molecule implosion and as a result – also for energy transferred onto the tube walls. The greatest reduction of cavitation index σ to -0.077 was recorded at contraction orifice radius r_1 = 0 mm and a water flow velocity of 100 m·s^{-1}. This shows that the degree of deformation for the water jet increases with an increase in flow velocity. A smaller decrease in cavitation index σ (-0.009) was observed for the simulation of water flow using an abstract model with tube contraction orifice edge radius r_3 = 2 mm.

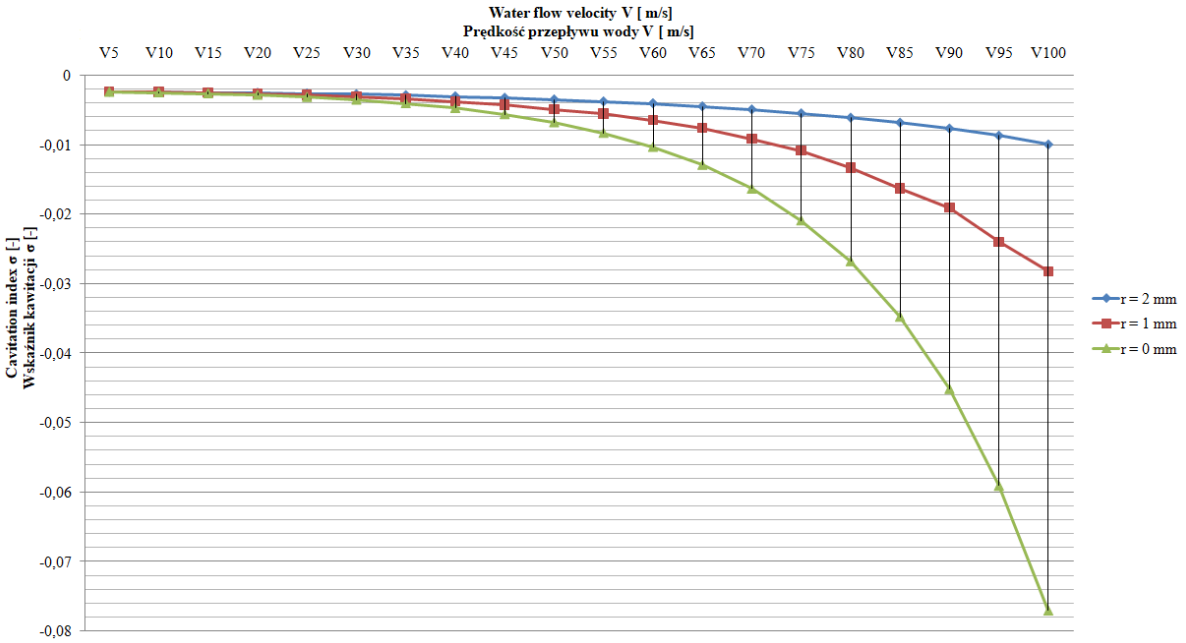

Source: own work / Źródło: opracowanie własne

Fig. 20. Values of cavitation index σ depending on water flow velocity and tube contraction orifice radius at the point with Cartesian system coordinates $x = 0$, $y = 0.05$, $z = 0.05$

Rys. 20. Wartości wskaźnika kawitacji σ w zależności od prędkości przepływu wody i promienia zaokrąglenia krawędzi zwężenia przewodu w punkcie o współrzędnych układu kartezjańskiego x = 0; y = 0,05; z = 0,05

4. Concluding remarks

Conducted simulation studies and the analysis of recorded results provide the foundations for the following conclusions:

1. Computer aided engineering systems (CAD/CAE) make it possible to modify the structure of a developed abstract system and real-time analysis of the effect of introduced changes in the geometry on parameters of flowing fluid.
2. Computer simulation of fluid flow and the development of abstract models of tubes facilitate research, as it reduced the time and costs connected with the construction of actual models.
3. It was found that a change in the tube contraction edge roundness affects kinematics and dynamics of fluid flow as well as changes in its parameters. This pertains primarily to fluid pressure, since it has a direct impact on the development of cavitation.
4. The performed simulation of fluid flow at the stage of tube construction makes it possible to identify areas at a particular risk of cavitation erosion. This facilitates the selection of geometrical dimensions of designed tubes and adequate structural materials.

5. References

[1] Behbahani-Nejad M., Changizian M:. Reduced-order modeling of three-dimensional unsteady partial cavity flows. Journal of Fluids and Structures, 2015, 52, 1–15.

[2] Brinkhorsta S., von Lavantea E., Wendtb G.: Experimental and numerical investigation of the cavitation-induced choked flow in a herschel venturi-tube. Flow Measurement and Instrumentation, 2017, 54, 56–67.

[3] Cioncolini A., Scenini F., Duff J., Szolcek M., Curioni M.: Experimental Thermal and Fluid Science Experimental Thermal and Fluid Science, 2016, 74, 49–57.

[4] Dular M., Griessler-Bulc T., Gutierrez-Aguirre I., Heath E., Kosjek T., Klemenćić A. K., Oder M., Petkovšek M., Raćki N., Ravnikar M., Šarc A., Širok B., Zupanc M., Zitnik M., Kompare B.: Use of hydrodynamic cavitation in (waste)water treatment. Ultrasonics Sonochemistry, 2016, 29, 577–588.

[5] Gao Sh., Zhao W., Lin H., Yang F., Chen X.: Feature suppression based CAD mesh model simplification. Computer-Aided Design, 2010, 42, 1178–1188.

[6] Hughes T.J.R., Cottrell J.A., Bazilevs Y.: Isogeometric analysis: CAD, finite elements, NURBS, exact geometry and mesh refinement. Comput. Methods Appl. Mech. Engrg., 2005, 194, 4135–4195.

[7] Lai Y., Hua S.-M., Martin R.R., Rosin P.L.: Rapid and effective segmentation of 3D models using random walks. Computer Aided Geometric Design, 2009, 26, 665–679.

[8] Lavoue G., Dupont F., Baskurt A.: A new CAD mesh segmentation method, based on curvature tensor analysis. Comput-Aided Des., 2005, 37(10), 975–87.

[9] Lee Y., Lee S., Shamir A., Cohen-Or D., Seidel H.: Mesh scissoring with minima rule and part salience. Computer Aided Geometric Design, 2005, 22, 444–465.

[10] Li D.G., Chen D.R., Liang P. Enhancement of cavitation erosion resistance of 316 L stainless steel by adding molybdenum. Ultrasonics Sonochemistry, 2017, 35, 375–381.

[11] Niederhofer P., Huth S., Theisen W.: Cavitation erosion and hydroabrasion resistance of cold work tool steels produced by powder metallurgy. Wear, 332-333, 2015, 1059–1069.

[12] Orzechowski Z., Prywer J., Zarzycki R.: Mechanika płynów w inżynierii środowiska. WNT Warszawa, 1997.

[13] Rockwella D., Lina J.-C., Oshkaia P., Reissa M., Pollack M.: Shallow cavity flow tone experiments: onset of locked-on states. Journal of Fluids and Structures, 2003, 17, 381–414.

[14] Steller K.: Pojęcia podstawowe ze szczególnym uwzględnieniem pojęć dotyczących maszyn hydraulicznych. Zeszyty Naukowe IMP PAN, 1982, 140.

[15] Steller K.: O mechanizmie niszczenia materiałów podczas kawitacji. Zeszyty Naukowe IMP PAN, 1983, 175.

[16] Sunil V.B., Pande S.S.: Automatic recognition of features from freeform surface CAD models. Computer-Aided Design, 2008, 40, 502–517.

[17] Thiruvegadam A.: On the modeling Cavitation Damage. Journal Ship Research, September 1969.

[18] Tran T.D., Nennemann B., Vu T.C. Guibault F.: Investigation of Cavitation Models for Steady and Unsteady Cavitating Flow Simulation. International Journal of Fluid Machinery and Systems, October-December 2015, Vol. 8 (4), 240–253.

[19] White D.R., Saigal S., Owen S.J.: Meshing complexity of single part CAD models. In: Proceedings of the 12th international meshing roundtable conference, 2003.

[20] Woo H., Kang E., Wang S., Lee K.H.: A new segmentation method for point cloud data. International Journal of Machine Tools & Manufacture, 2002, 42. 167–178.

[21] Wójs K.: Kawitacja w cieczach o różnych właściwościach reologicznych. Oficyna Wydawnicza Politechniki Wrocławskiej, Wrocław 2004.

[22] Varady T., Facello M.A., Terek Z.: Automatic extraction of surface structures in digital shape reconstruction. Computer-Aided Design, 2007, 39, 379–388.

[23] Vu T., Koller M., Gauthier M., Deschênes C.: Flow simulation and efficiency hill chart prediction for a Propeller turbine. International Journal of Fluid Machinery and Systems, April-June 2011, Vol. 4(2), 243–254.

[24] Xiao D., Lin H., Xian Ch., Gao Sh.: CAD mesh model segmentation by clustering. Computers and Graphics, 2011, 35, 685–691.

[25] Zhang Y.-Y., Sun X.-J., Huang D.-G.: A Numerical Study on Cavitation Suppression Using Local Cooling. International Journal of Fluid Machinery and Systems, October-December 2010, Vol. 3(4), 292–300.

[26] Zhu L., Li., Martin R.R.: Direct simulation for CAD models undergoing parametric modifications. Computer-Aided Design, 2016, 78, 3–13.